IMPLEMENTATION OF A NEW THERMO-VISCOPLASTIC SOIL MODEL USING FENICS PLATFORM

X. Cheng[1], Y. Li[2], M. Karstunen[3], J. Dijkstra[4] and A. Abed[5]

KEYWORDS

FEM, THM coupling, Thermal viscoplasticity, FEniCS.

ABSTRACT

The heating and cooling processes (e.g., imposed by energy geostructures) may cause undesired displacement of soil, which in turn may impact the long-term stability of the geothermal structures. This is true especially those installed in sensitive clays due to the high dependence of their creep behaviour on the temperature. This paper presents a numerical implementation algorithm for an enhancement of an existing hydro-mechanical model into a Finite Element code based on FEniCS platform. It also includes a validation example against experimental data of thermal oedometer tests. The quantitative comparison to experimental results supported the suitability of the framework.

1. EXAMPLE INTRODUCTION

The rapid expansion of the energy geotechnics sector has driven the wide recognition of the influence of temperature on the behaviour of geomaterials. Thus, it is generally acknowledged that the volumetric behaviour, creep rate, shear strength and pore water pressure of clay are temperature dependent.

[1] Department of Architecture and Civil Engineering, Chalmers University of Technology, Gothenburg, Sweden
[2] NCC Teknik, NCC Sverige AB, Gothenburg, Sweden
[3] Department of Architecture and Civil Engineering, Chalmers University of Technology, Gothenburg, Sweden
[4] Department of Architecture and Civil Engineering, Chalmers University of Technology, Gothenburg, Sweden
[5] Department of Architecture and Civil Engineering, Chalmers University of Technology, Gothenburg, Sweden

Given the complexity of the thermal behaviour, it is necessary to enhance the understanding of the fundamental mechanisms of the coupled Thermo-Hydro-Mechanical (THM) behaviour to satisfactorily predict the response of the geostructures concerned.

The response of geostructures, has been recently successfully simulated [1], [2], [3] , thanks to the development of THM framework [4], [5], [6], [7] . Most of these numerical codes are not easy to access and vary in complexity, which poses challenges to their applications to specific problems based on the needs of the user.

In addition, modelling such intricate physical processes requires robust constitutive relationships. A variety of constitutive models focusing on the temperature dependent yield surface (e.g. [8], [9], [10]) have been developed. However, to date most constitutive models were developed in the context of nuclear waste barriers involving significant temperature variation, whereas the creep mechanism of sensitive clay under modest temperature changes, commonly the case in Canada and Scandinavia, is not yet well understood. In this respect, informed by a systematic series of thermal oedometer tests, Li [11] proposed a thermo-viscoplastic soil model, in which thermo-mechanical behaviour is incorporated using a temperature and creep rate dependent yield surface.

Following the work of [12] [13] , this paper aims to provide a reliable computational framework combining a THM coupling and aforementioned thermal constitutive model [11] using the FEniCS platform [14] .

2. GOVERNING BALANCE EQUATIONS

This section briefly presents the governing balance equations regarding mass, energy and mechanics with assumptions: (1) the porous geomaterial consists of three phases - liquid (l), gas (g) and solid (s); (2) solid phase does not dissolve or sublimate while water may transform between vapour and liquid; (3) dry air is not considered.

2.1 Water mass balance equation

The mass balance equation for water component is presented by:

$$
\begin{aligned}
&[n(\rho_w^l - \rho_w^g)\frac{\delta S^l}{\delta T} - (1-n)(S^l\rho_w^l + S^g\rho_w^g)\beta_{sT} - nS^l\beta_{wT}\rho_w^l \\
&\qquad + nS^g\frac{\rho_w^g}{T^2}(4974 + \frac{M_w \mathrm{s}}{R\rho_w^l})]\frac{\partial T}{\partial t} \\
&+[nS^l\beta_{wp}\rho_w^l + nS^g\frac{\rho_w^g M_w}{\rho_w^l RT} - n(\rho_w^l - \rho_w^g)\frac{\partial S^l}{\partial \mathrm{s}}]\frac{\partial u_w}{\partial t} \\
&+(S^l\rho_w^l + S^g\rho_w^g)\frac{\partial \varepsilon_v}{\partial t} + \boldsymbol{\nabla}\cdot[\frac{\rho_w^l K_w}{\rho_w^l g}(\nabla u_w + \rho_w^l g)] = 0
\end{aligned}
\qquad (1)
$$

where n is the soil porosity, ρ_w^l is the water density in a liquid phase dependent on the pore pore-water pressure u_w and the temperature T, ρ_w^g is the vapour density in a gas phase. S^l and S^g are the degree of saturation for liquid and gas, respectively, where S^l is assumed to be a function of suction (s) for unsaturated soil [15]. β_{sT} and β_{wT} are the coefficients of volumetric thermal expansion in solids and water respectively. M_w is the molar mass of vapour and R is the universal gas constant. β_{wp} is the coefficient of water compressibility, ε_v is the volumetric strain. K_w denotes hydraulic conductivity of liquid water. g is gravity acceleration.

2.2 Energy balance equation

The energy balance equation considering the latent heat of vaporization and heat due to conduction and convection can be expressed as:

$$
\underbrace{\frac{\partial \Phi_h}{\partial t}}_{\text{heat storage}} + \underbrace{LQ_w^g}_{\text{latent heat of vaporization}} + \underbrace{\boldsymbol{\nabla}\cdot\mathbf{q_h}}_{\text{heat due to conduction and convection}} = 0 \qquad (2)
$$

with

$$
\Phi_h = [(1-n)\rho^s c_s + nS^l\rho_w^l c_w^l + nS^g\rho_w^g c_w^g](T - T_0) \qquad (3)
$$

$$
Q_w^g = -(1-n)S^g\rho_w^g\beta_{sT}\frac{\partial T}{\partial t} + S^g\rho_w^g\frac{\partial \varepsilon_v}{\partial t} - n\rho_w^g\frac{\partial S^l}{\partial t} + nS^g\frac{\partial \rho_w^g}{\partial t} \qquad (4)
$$

$$
\mathbf{q}_\mathrm{h} = -\lambda_T\nabla T + \frac{\rho_w^l c_w^l K_w}{\rho_w^l g}(\nabla u_w + \rho_w^l g)(T - T_0) \qquad (5)
$$

where λ_T is the thermal conductivity. T_0 is the reference temperature with a value of 293.16 K for this research. L is the latent heat of water vaporization.

2.3 Mechanical balance equation

The mechanical balance equation is given by:

$$\nabla \cdot \boldsymbol{\sigma}^{\mathrm{tot}} + \rho^b \mathbf{g} = 0 \qquad (6)$$

where $\boldsymbol{\sigma}^{tot}$ is the total stress tensor, $\rho^b \mathbf{g}$ is body force that typically denotes self-weight of material related to its bulk density.

The corresponding weak formulation of the balance equations (Eqs. (1), (2) and (*6*)) can be derived by multiplying the corresponding independent test functions $\mathbf{X} = [\delta u, \delta u_w, \delta T]$ and integrating over the spatial domain Ω, where the symbols δu, δu_w and δT are the variations in nodal displacements, water pressure and temperature, respectively. The full details are described in [12].

3. CREEP-SCLAY1ST

Stress integration relies largely on the constitutive model that describes the stress strain response of material. This section summarizes key aspects of an enhanced version of Creep-SCLAY1S model [16] , namely Creep-SCLAY1ST [11] , which is capable of capturing the bonding-dependent thermal softening and hardening of the natural sensitive clay. In what follows, for the sake of simplicity, the model will be discussed assuming triaxial stress state, however, the actual implementation is done with the generalized version.

Following the elasto-plasticity theory, the total strain rate $\dot{\varepsilon}$ in Creep-SCLAY1ST that accounts for thermal effects is expressed as follows:

$$\dot{\boldsymbol{\varepsilon}} = \dot{\boldsymbol{\varepsilon}}_{\sigma}^{e} + \alpha_T \dot{T} \boldsymbol{\delta}_{ij} + \dot{\boldsymbol{\varepsilon}}^{vp} \qquad (7)$$

where $\dot{\boldsymbol{\varepsilon}}_{\sigma}^{e}$, $\alpha_T \dot{T} \boldsymbol{\delta}_{ij}$ and $\dot{\boldsymbol{\varepsilon}}^{vp}$ are vectors of mechanical elastic strains, thermal expansion and viscoplastic strain, respectively. α_T is the thermal expansion coefficient. $\boldsymbol{\delta}_{ij}$ is the vector {1, 1, 1, 0, 0, 0} indicating that the model assumes that temperature contributes to volumetric strains only.

Similarly to Creep-SCLAY1S model, three surfaces with similar sheared ellipse in triaxial stress plane, namely the Normal Compression Surface (NCS), the Current Stress Surface (CSS) and the Imaginary Intrinsic Compression Surface (ICS) [17][18] , are used to represent the stress state and bonding amount of the model (Figure 1). Their sizes are defined by the intersection of the vertical tangent to the ellipse with the mean effective stress axis p'_m, p'_{eq} and p'_{mi}, respectively - e.g. Eq (*8*):

$$p'_m = p' + \frac{(q - \alpha p')^2}{(M^2(\theta_\alpha) - \alpha^2)p'} \qquad (8)$$

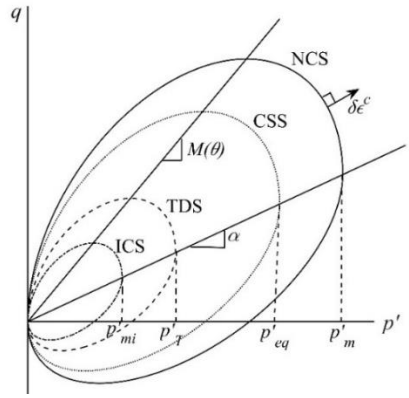

Figure 1 Description of the main characteristics of Creep-SCLAY1ST in the p'- q plane.

where p' is the mean effective stress, q is the deviatoric stress, α is a state variable related to the inclination of the yield surface, $M(\theta_\alpha)$ is Lode angle θ_α dependent stress ratio at critical state (details see [19]). The NCS and ICS can be linked by the amount of natural bonding (χ):

$$p'_m = p'_{mi}(1+\chi) \quad (9)$$

A novel development of Creep-SCLAY1ST relates to the introduction of an additional temperature-dependent surface – TDS, by incorporating the effect of the temperature (T) and the initial amount of natural bonding (χ_0):

$$\frac{p'_T}{p'_{mi}} = \left(\frac{T}{T_{ref}}\right)^{-(a_T\chi_0+b_T)} \quad (10)$$

where a_T and b_T are material specific thermal factors. Eq (*9*) is therefore updated with p'_T to obtain a temperature dependent preconsolidation pressure:

$$p'_m = p'_T(1+\chi) \quad (11)$$

Such an update induces the shrinking of the NCS during heating (i.e., thermal softening) and its expansion during cooling. The Creep-SCLAY1ST model comprises three hardening laws, in which isotropic hardening (Eq. (*12*)) and destructuration (Eq. (*14*)) will affect the size of TDS and NCS, and rotational hardening (Eq. (*13*)) will affect the orientation of TDS, CSS and NCS. It is worth noting that isotropic hardening evolves as a function of both volumetric creep strains ($\dot{\varepsilon}_v^c$) and temperature ($\dot{T}$) rates, while the rest of the hardening laws remain the same as that for Creep-SCLAY1S model:

$$\dot{p}'_T = \frac{p'_T}{\lambda^* - \kappa^*}\dot{\varepsilon}^c_v - (\mathrm{a_T}\chi_0 + b_T)p'_T(\frac{\dot{T}}{T}) \quad (12)$$

$$\delta\alpha = \omega([\frac{3\eta}{4} - \alpha]\langle\delta\varepsilon^c_v\rangle + \omega_d[\frac{\eta}{3} - \alpha]|\delta\varepsilon^c_q|) \quad (13)$$

$$\dot{\chi} = -\xi\chi(|\dot{\varepsilon^c_v}| + \xi_d|\dot{\varepsilon^c_q}|) \quad (14)$$

where λ^* is the modified intrinsic compression index, and $\kappa^*$is the modified swelling index. η is the stress ratio and ω and ω_d are model constants associated with the evolution of anisotropy. ξ and ξ_d are model parameters related to the bond degradation. The volumetric ($\dot{\varepsilon}^c_v$) and deviatoric ($\dot{\varepsilon}^c_q$) creep strain rates in Eqs. (*15*) and (*16*) are calculated using the concept of a viscoplastic multiplier $\dot{\Lambda}$ expressed by Eq. (*17*) [19]:

$$\dot{\varepsilon}^c_v = \dot{\Lambda}\frac{\partial p'_{eq}}{\partial p'} \quad (15)$$

$$\dot{\varepsilon}^c_q = \dot{\Lambda}\frac{\partial p'_{eq}}{\partial q} \quad (16)$$

with

$$\dot{\Lambda} = \frac{\mu^*_i}{\tau}(\frac{p'_{eq}}{p'_m})^\beta(\frac{M^2_c - \alpha^2_{K^{nc}_0}}{M^2_c - \eta^2_{K^{nc}_0}}) \quad (17)$$

and

$$\beta = \frac{\lambda^* - \kappa^*}{\mu^*_i} \quad (18)$$

where μ^*_i is the intrinsic creep index, and τ is the reference time.

4. NUMERICAL IMPLEMENTATION AND VALIDATION

The coupled THM balance equations combined with the Creep-SCLAY1ST model were scripted using Python and ran using the open source FEniCS platform. The following section presents the validation of the model results against experimental observations from thermally controlled oedometer tests.

4.1 Numerical model

The proposed framework was verified against the experimental test results on Utby clay reported in [11]. A three-dimensional finite element model was established to simulate the oedometer tests, as illustrated in Figure 2. The geometry of the FE model with a height of 18 mm and diameter of 50 mm, is discretized with 496 tetrahedra elements with 4 Gauss points associated with each element.

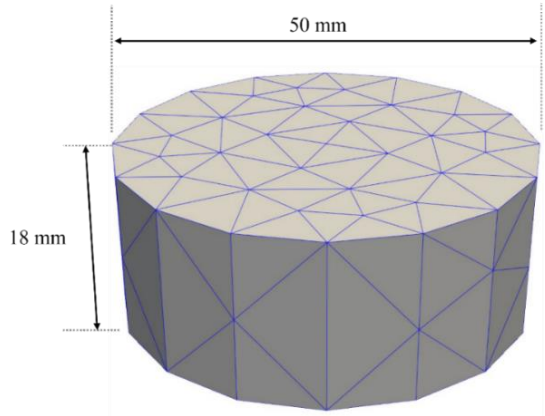

Figure 2 Representative mesh used in the simulations.

The imposed boundary conditions in the model are as follows:

- The displacement boundary conditions include the restriction of movements in all directions at the bottom, while the displacements perpendicular to the cylindrical boundary are also set to zero. The top surface is set to move freely.
- The hydraulic boundary conditions are prescribed as impermeable at the top and the cylindrical boundaries of the mesh, whereas no change in the pore water pressure from the initial condition is set to the bottom surface for a drained condition.
- A closed form of temperature boundary condition is deployed on bottom and cylindrical boundaries of the mesh, while a time-dependent temperature is prescribed to the top boundary to simulate the heating or cooling of the sample. Note that the temperature imposed in the top boundary can spread to the whole sample within a short time owing to the small size of the sample.

The mechanical parameters of Creep-SCLAY1ST model in Table 1 were adopted for the numerical simulation. A total of 18 model parameters are involved. 14 of them, which were previously introduced in the Creep-SCLAY1S, have been kept identical to the ones calibrated and reported following [16]. The 4 thermal parameters are then derived according to the experimental fit.

Table 1. Parameters for Utby clay.

e_0	ν'	OCR	λ*	κ*	M_c	M_e
1.97	0.2	1.2	0.0862	0.0083	1.45	1.1
μ*	T (day)	α_0	ω	ω_d	χ_0	ξ_d
0.004	1	0.5	40	0.9	6	0.3
ξ	α_T (1/K)	T_{ref} (°C)	a_T	b_T		
9	3.2e-5	7	8.5e-3	5.1e-3		

4.2 Loading scenarios

Herein, 4 tests from Li's experiments [11], including two loading paths O_1 and O_2 under either a cooling or heating process, on intact samples with an initial void ratio equal to 1.97 from 6 m depth were selected to check the capabilities of the proposed model, as shown in Figure 3. All samples were initially loaded to the estimated in-situ vertical effective stress level of 45 kPa under temperature T1, and then the loading procedure shown in Figure 3 proceeded by bringing the samples to 6 different stress levels σ_v'. The temperature of the sample also varied at each stress level. Details of the selected tests are given in Table 2, where the test step, duration of each step, vertical stress level and temperature are provided.

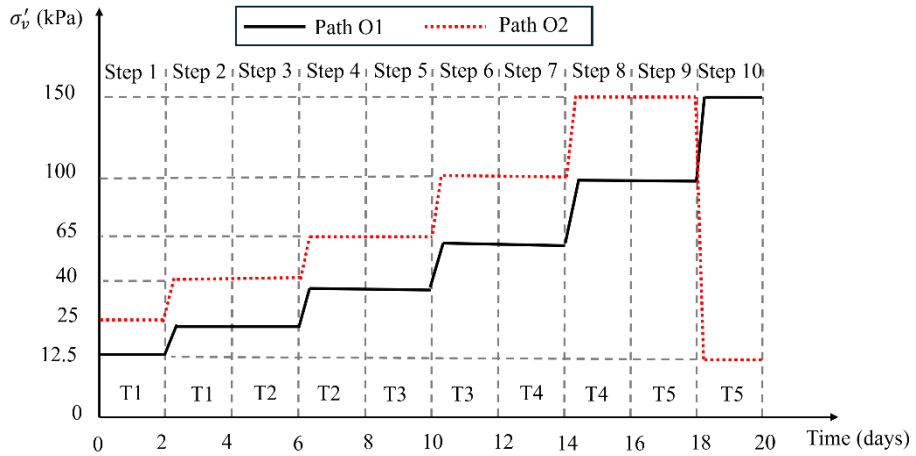

Figure 3 Schematic of the test procedure.

4.3 Results

The curves regarding void ratio (e) against vertical effective stress (σ_v') in logarithm obtained from numerical analysis with Creep-SCLAY1ST and Creep-SCLAY1S models and experimental observation are plotted in Figure 4a and c. It is apparent that the overall mechanical behaviour is reasonably well captured by Creep-SCLAY1ST and Creep-SCLAY1S models for the two loading paths under heating and cooling processes. However, the Creep-SCLAY1S model seems unable to reproduce the variation of preconsolidation pressure

under thermal loading. For Creep-SCLAY1ST model, as expected, an increase trend of the preconsolidation pressure was observed in the cooling process, while the heating process causes the decrease in preconsolidation pressure.

Table 2. Selected tests for numerical simulations.

Step	Time (days)	Temperature T (°C)			Stress σ'_v (kPa)	
		Cooling	T	Heating	O_1	O_2
1	2	5	T1	25	12.5	25
2	2	5	T1	25	25	40
3	2	10	T2	20	25	40
4	2	10	T2	20	40	65
5	2	15	T3	15	40	65
6	2	15	T3	15	65	100
7	2	20	T4	10	65	100
8	2	20	T4	10	100	150
9	2	25	T5	5	100	150
10	2	25	T5	5	150	12.5

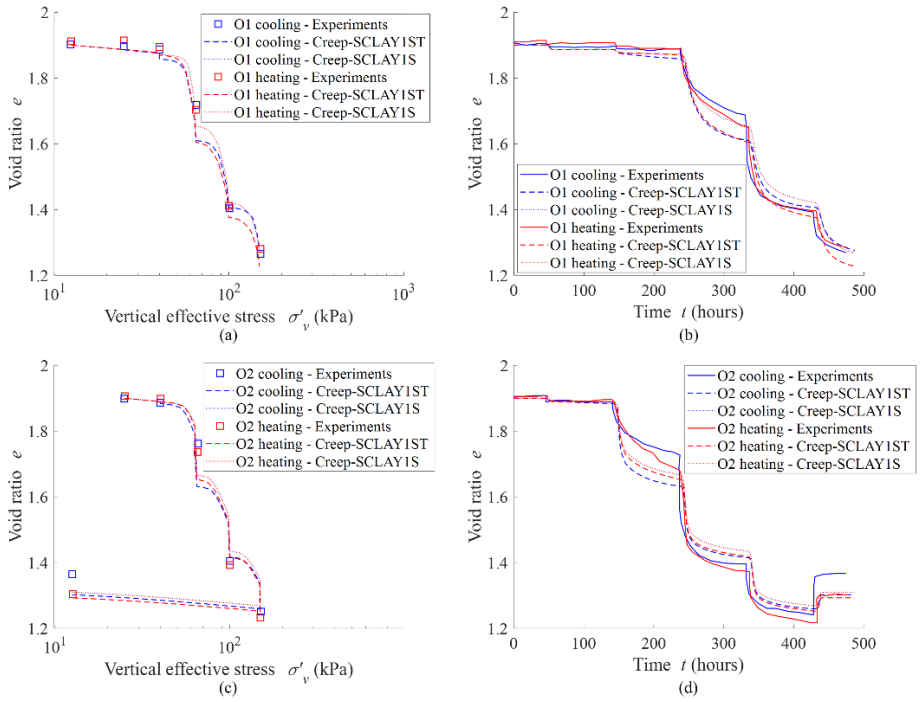

Figure 4 Compression curves (a) for loading path O1 and (c) for loading path O2 and the time-void ratio curves (b) for loading path O1 and (d) for loading path O2. note O1 and O2 cooling/heating Creep-SCLAY1S curves overlapped.

The variations of void ratio in Figure 4b and d again show overall encouraging results regarding the performance of Creep-SCLAY1ST and Creep-

SCLAY1S models when compared with experimental results, although a slight overestimation of the decrease in void ratio when samples are loaded beyond their respective preconsolidation pressures (Step 4).

It is worthwhile to investigate the influence of temperature on deformation of the clay under constant stress level. Figure 5 shows the variation of void ratio under vertical stress of 65 kPa at step 7 in loading path O_1, where the intact clay samples with identical stress histories are thermally loaded from an equal temperature for heating (15 °C to 20 °C) and cooling (15 °C to 10 °C). The experimental results indicate that larger compression is induced by heating than by cooling due to the heating softening. Such phenomenon is better reproduced by Creep-SCLAY1ST, while no difference was observed between heating and cooling in the results by Creep-SCLAY1S.

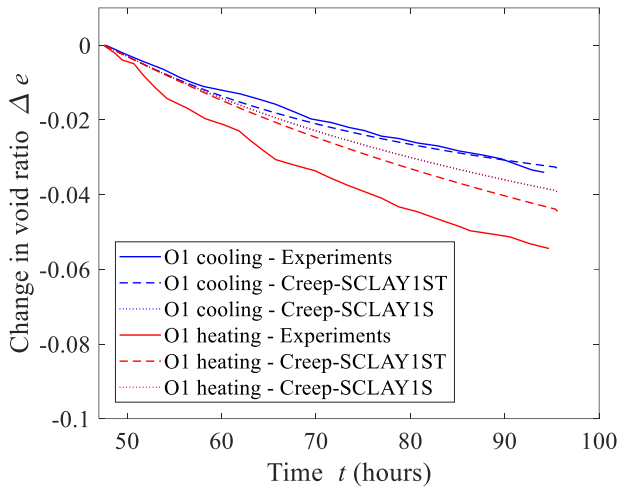

Figure 5 Change in void ratio under temperature change with 5°C under stress level of 65 kPa for O1 stress paths. note O1 cooling/heating Creep-SCLAY1S curves are overlapped.

5. CONCLUSIONS

This paper presented an implementation of a new thermo-viscoplastic constitutive model into a coupled THM framework based on FEniCS platform. The proposed constitutive model improves the thermal performance of Creep-SCLAY1S by introducing an additional temperature and creep rate dependent surface to keep track of the variation of preconsolidation pressure induced by the thermal loading. The model results were validated by simulating results of oedometer tests on soft soil under combined mechanical and thermal loading conditions. The results highlighted the potential of the model and the computational framework to accurately predict the thermal response of intact sensitive clay, as well as to be employed in the simulation of thermal related geotechnical problems.

ACKNOWLEDGEMENT

The work is funded by Formas (Research Council for sustainable Development, Grant (2021-02400) and Swedish Transport Administration (Grant 2022/69758) via BIG (Branchsamverkan in grunden). The work is done as part of Digital Twin Cities Centre that is supported by Sweden's Innovation Agency VINNOVA (Grant 2019-00041).

REFERENCES

[1] Di Donna, A., Loria, A.F.R. and Laloui, L.: Numerical study of the response of a group of energy piles under different combinations of thermo-mechanical loads. Computers and Geotechnics, 72, pp.126-142, 2016.

[2] Gawecka, K.A., Taborda, D.M., Potts, D.M., Cui, W., Zdravković, L. and Haji Kasri, M.S.: Numerical modelling of thermo-active piles in London Clay. Proceedings of the Institution of Civil Engineers-Geotechnical Engineering, 170(3), pp.201-219, 2017.

[3] Liu, R.Y.W., Sailer, E., Taborda, D.M., Potts, D.M. and Zdravković, L.: A practical method for calculating thermally-induced stresses in pile foundations used as heat exchangers, Computers and Geotechnics, 126, p.103743, 2020.

[4] Schrefler, B.A., Zhan, X. and Simoni, L.: A coupled model for water flow, airflow and heat flow in deformable porous media. International Journal of Numerical Methods for Heat & Fluid Flow, 5(6), pp.531-547, 1995.

[5] Collin, F., Li, X.L., Radu, J.P. and Charlier, R.: Thermo-hydro-mechanical coupling in clay barriers. Engineering Geology, 64(2-3), pp.179-193, 2002.

[6] Gens, A., Guimaräes, L.D.N., Olivella, S. and Sánchez, M.J.J.O.R.M.: Modelling thermo-hydro-mechano-chemical interactions for nuclear waste disposal. Journal of Rock Mechanics and Geotechnical Engineering, 2(2), pp.97-102, 2010.

[7] Cui, W.: Development, implementation and application of thermo-hydro-mechanical coupling for soils in finite element analysis. PhD thesis, Imperial College London, 2015.

[8] Abuel-Naga, H.M., Bergado, D.T., Bouazza, A. and Pender, M.: Thermomechanical model for saturated clays. Géotechnique, 59(3), pp.273-278, 2009.

[9] Cui, Y.J., Sultan, N. and Delage, P.: A thermomechanical model for saturated clays. Canadian Geotechnical Journal, 37(3), pp.607-620, 2000.

[10] Laloui, L. and François, B.: ACMEG-T: soil thermoplasticity model. Journal of engineering mechanics, 135(9), pp.932-944, 2009.

[11] Li, Yanling.: On the impact of temperature perturbations on the creep of sensitive clay. PhD thesis, Chalmers University of Technology, 2019.

[12] Abed, A.A. and Sołowski, W.T.: A study on how to couple thermo-hydro-mechanical behaviour of unsaturated soils: Physical equations, numerical implementation and examples. Computers and Geotechnics, 92, pp.132-155, 2017.

[13] Abed, A., Gerolymato, E., Karstunen, M.: FEniCS simulation of a partially saturated slope under varying environmental loads. In Proceedings 10th European Conference on Numerical Methods in Geotechnical Engineering (London), 2023.

[14] Logg, A., Mardal, K.-A., Wells, G. Automated solution of differential equations by the finite element method: The FEniCS book. Springer Science & Business Media, 2012.

[15] Srivastava, R. and Yeh, T.C.J.: Analytical solutions for one-dimensional, transient infiltration toward the water table in homogeneous and layered soils. Water Resources Research, 27(5), pp.753-762, 1991.

[16] Gras, J.-P., Sivasithamparam, N., Karstunen, M., Dijkstra, J.: Permissible range of model parameters for natural fine-grained materials. Acta Geotechnica, 13(2), 387-398, 2018.

[17] Gens, A., Nova, R.: Conceptual bases for a constitutive model for bonded soils and weak rocks. In: Geomechanical Engineering of Hard Soils and Soft Rocks. (Eds: A. Anagnostopoulos, F. Schlosser, N. Kaltesiotis, & R. Frank), Vol. 1, pp. 485–494, A.A. Balkema, Rotterdam, 1993.

[18] Karstunen, M., Krenn, H., Wheeler, S. J. Koskinen, M., Zentar, R. Effect of anisotropy and destructuration on the behaviour of Murro test embankment. International Journal of Geomechanics 5 (2): 87-97, 2005.

[19] Sivasithamparam, N., Karstunen, M., Bonnier, P.: Modelling creep behaviour of anisotropic soft soils. Computers and Geotechnics 69, 46-57, 2015.